LECTURE 18: Horn Antennas

(*Rectangular horn antennas*. *Circular apertures*.)

1 Rectangular horn antennas

Horn antennas are popular in the microwave band (above 1 GHz). Horns provide high gain, low VSWR (with waveguide feeds), relatively wide bandwidth, and they are not difficult to make. There are three basic types of rectangular horns.

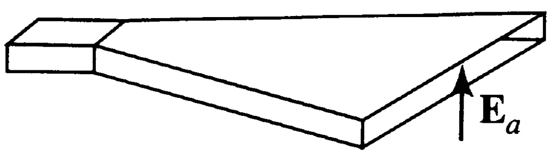

(a) H-plane sectoral horn.

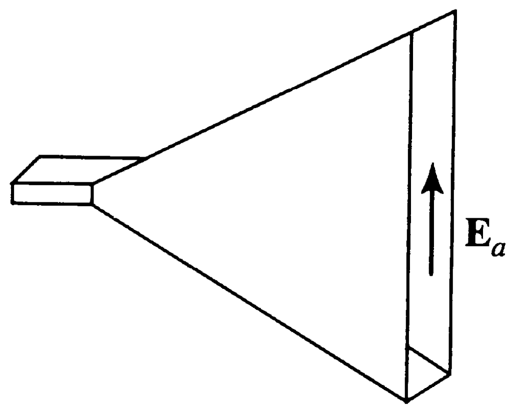

(b) E-plane sectoral horn.

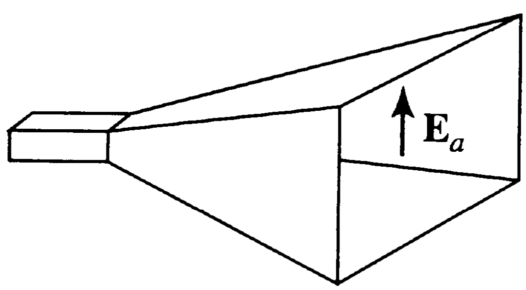

(c) Pyramidal horn.

The horns can be also flared exponentially. This provides better matching in a broad frequency band, but is technologically more difficult and expensive.

The rectangular horns are ideally suited for rectangular waveguide feeders. The horn acts as a gradual transition from a waveguide mode to a free-space mode of the EM wave. When the feeder is a cylindrical waveguide, the antenna is usually a ***conical horn***.

Why is it necessary to consider the horns separately instead of applying the theory of waveguide aperture antennas directly? It is because the so-called ***phase error*** occurs due to the difference between the lengths from the center of the feeder to the center of the horn aperture and the horn edge. This makes the uniform-phase aperture results invalid for the horn apertures.

1.1 The *H*-plane sectoral horn

The geometry and the respective parameters shown in the figure below are used often in the subsequent analysis.

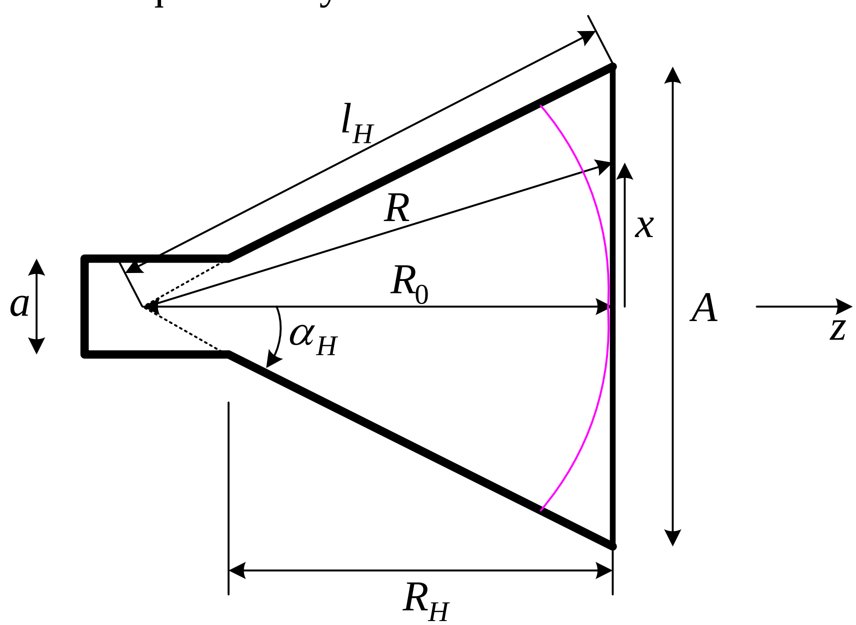

H-plane (*x*-*z*) cut of an *H*-plane sectoral horn

$$l_H^2 = R_0^2 + \left(\frac{A}{2}\right)^2, \tag{18.1}$$

$$\alpha_H = \arctan\left(\frac{A}{2R_0}\right), \tag{18.2}$$

$$R_H = (A-a)\sqrt{\left(\frac{l_H}{A}\right) - \frac{1}{4}}. \tag{18.3}$$

The two fundamental dimensions for the construction of the horn are A and R_H.

The tangential field arriving at the input of the horn is composed of the transverse field components of the waveguide dominant mode TE_{10}:

$$\left| \begin{array}{l} E_y = E_0 \cos\left(\frac{\pi}{a}x\right) e^{-j\beta_g z} \\ H_x = -E_y / Z_g \end{array} \right. \tag{18.4}$$

where

$Z_g = \dfrac{\eta}{\sqrt{1-\left(\frac{\lambda}{2a}\right)^2}}$ is the wave impedance of the TE_{10} mode;

$\beta_g = \beta_0 \sqrt{1-\left(\frac{\lambda}{2a}\right)^2}$ is the propagation constant of the TE_{10} mode.

Here, $\beta_0 = \omega\sqrt{\mu\varepsilon} = 2\pi/\lambda$, and λ is the free-space wavelength. The field that is illuminating the aperture of the horn is essentially an expanded version of the waveguide field. Note that the wave impedance of the flared waveguide (the horn) gradually approaches the intrinsic impedance of open space η, as A (the *H*-plane width) increases.

The complication in the analysis arises from the fact that the waves arriving at the horn aperture are ***not in phase*** due to the different path lengths from the horn apex. The aperture phase variation is given by

$$e^{-j\beta(R-R_0)}. \tag{18.5}$$

Since the aperture is not flared in the *y*-direction, the phase is uniform in this direction. We first approximate the path of the wave in the horn:

$$R = \sqrt{R_0^2 + x^2} = R_0\sqrt{1+\left(\frac{x}{R_0}\right)^2} \approx R_0\left[1+\frac{1}{2}\left(\frac{x}{R_0}\right)^2\right]. \tag{18.6}$$

The last approximation holds if $x \ll R_0$, or $A/2 \ll R_0$. Then, we can assume that

$$R - R_0 \approx \frac{1}{2}\frac{x^2}{R_0}. \tag{18.7}$$

Using (18.7), the field at the aperture is approximated as

$$E_{a_y} = E_0 \cos\left(\frac{\pi}{A}x\right) e^{-j\frac{\beta}{2R_0}x^2}. \tag{18.8}$$

The field at the aperture plane outside the aperture is assumed equal to zero. The field expression (18.8) is substituted in the integral I_y^E (see Lecture 17):

$$I_y^E = \iint_{S_A} E_{a_y}(x', y') e^{j\beta(x'\sin\theta\cos\varphi + y'\sin\theta\sin\varphi)} dx'dy', \tag{18.9}$$

$$I_y^E = E_0 \underbrace{\int_{-A/2}^{+A/2} \cos\left(\frac{\pi}{A}x'\right) e^{-j\frac{\beta}{2R_0}x'^2} e^{j\beta x'\sin\theta\cos\varphi} dx'}_{\sim I(\theta,\varphi)} \times \int_{-b/2}^{+b/2} e^{j\beta y'\sin\theta\sin\varphi} dy'. \tag{18.10}$$

The second integral has been already encountered. The first integral is cumbersome and the final result only is given below:

$$I_y^E = E_0 \left[\frac{1}{2}\sqrt{\frac{\pi R_0}{\beta}} \cdot I(\theta,\varphi)\right] \times \left[b \frac{\sin\left(\frac{\beta b}{2}\sin\theta\sin\varphi\right)}{\frac{\beta b}{2}\sin\theta\sin\varphi} \right], \tag{18.11}$$

where

$$\begin{aligned} I(\theta,\varphi) = {} & e^{j\frac{R_0}{2\beta}\left(\beta\sin\theta\cos\varphi + \frac{\pi}{A}\right)^2} \cdot \left[C(s_2') - jS(s_2') - C(s_1') + jS(s_1')\right] \\ & + e^{j\frac{R_0}{2\beta}\left(\beta\sin\theta\cos\varphi - \frac{\pi}{A}\right)^2} \cdot \left[C(t_2') - jS(t_2') - C(t_1') + jS(t_1')\right] \end{aligned} \tag{18.12}$$

and

$$s_1' = \sqrt{\frac{1}{\pi\beta R_0}} \left(-\frac{\beta A}{2} - R_0\beta u - \frac{\pi R_0}{A} \right);$$

$$s_2' = \sqrt{\frac{1}{\pi\beta R_0}} \left(+\frac{\beta A}{2} - R_0\beta u - \frac{\pi R_0}{A} \right);$$

$$t_1' = \sqrt{\frac{1}{\pi\beta R_0}}\left(-\frac{\beta A}{2} - R_0\beta u + \frac{\pi R_0}{A}\right);$$

$$t_2' = \sqrt{\frac{1}{\pi\beta R_0}}\left(+\frac{\beta A}{2} - R_0\beta u + \frac{\pi R_0}{A}\right);$$

$$u = \sin\theta\cos\varphi.$$

$C(x)$ and $S(x)$ are Fresnel integrals, which are defined as

$$C(x) = \int_0^x \cos\left(\frac{\pi}{2}\tau^2\right)d\tau; \quad C(-x) = -C(x),$$
$$S(x) = \int_0^x \sin\left(\frac{\pi}{2}\tau^2\right)d\tau; \quad S(-x) = -S(x). \tag{18.13}$$

More accurate evaluation of I_y^E can be obtained if the approximation in (18.6) is not made, and E_{a_y} is substituted in (18.9) as

$$E_{a_y} = E_0\cos\left(\frac{\pi}{A}x\right)e^{-j\beta\left(\sqrt{R_0^2+x^2}-R_0\right)} = E_0 e^{+j\beta R_0}\cos\left(\frac{\pi}{A}x\right)e^{-j\beta\sqrt{R_0^2+x^2}}. \tag{18.14}$$

The far field can be now calculated as (see Lecture 17):

$$E_\theta = j\beta\frac{e^{-j\beta r}}{4\pi r}(1+\cos\theta)\sin\varphi\cdot I_y^E,$$
$$E_\varphi = j\beta\frac{e^{-j\beta r}}{4\pi r}(1+\cos\theta)\cos\varphi\cdot I_y^E, \tag{18.15}$$

or

$$\mathbf{E} = j\beta E_0 b\sqrt{\frac{\pi R_0}{\beta}}\frac{e^{-j\beta r}}{4\pi r}\left(\frac{1+\cos\theta}{2}\right)\left[\frac{\sin\left(\frac{\beta b}{2}\sin\theta\sin\varphi\right)}{\frac{\beta b}{2}\sin\theta\sin\varphi}\right]\times$$
$$I(\theta,\varphi)\left(\hat{\boldsymbol{\theta}}\sin\varphi + \hat{\boldsymbol{\varphi}}\cos\varphi\right). \tag{18.16}$$

The amplitude pattern of the *H*-plane sectoral horn is obtained as

$$\bar{E} = \left(\frac{1+\cos\theta}{2}\right) \cdot \left[\frac{\sin\left(\frac{\beta b}{2}\sin\theta\sin\varphi\right)}{\frac{\beta b}{2}\sin\theta\sin\varphi}\right] \cdot I(\theta,\varphi). \tag{18.17}$$

<u>Principal-plane patterns</u>

***E*-plane** ($\varphi = 90°$): $F_E(\theta) = \left(\frac{1+\cos\theta}{2}\right)\left[\frac{\sin\left(\frac{\beta b}{2}\sin\theta\sin\varphi\right)}{\frac{\beta b}{2}\sin\theta\sin\varphi}\right]$ (18.18)

It can be shown that the second factor in (18.18) is exactly the pattern of a uniform line source of length *b* along the *y*-axis.

***H*-plane** ($\varphi = 0^\circ$):

$$\begin{aligned} F_H(\theta) &= \left(\frac{1+\cos\theta}{2}\right) \cdot f_H(\theta) = \\ &= \left(\frac{1+\cos\theta}{2}\right) \cdot \frac{I(\theta,\varphi=0°)}{I(\theta=0°,\varphi=0°)} \end{aligned} \tag{18.19}$$

The *H*-plane pattern in terms of the $I(\theta,\varphi)$ integral is an approximation, which is a consequence of the phase approximation made in (18.7). Accurate value for $f_H(\theta)$ is found by integrating numerically the field as given in (18.14), i.e.,

$$f_H(\theta) \propto \int_{-A/2}^{+A/2} \cos\left(\frac{\pi x'}{A}\right) e^{-j\beta\sqrt{R_0^2+x'^2}} e^{j\beta x'\sin\theta} dx'. \tag{18.20}$$

E- AND H-PLANE PATTERN OF H-PLANE SECTORAL HORN

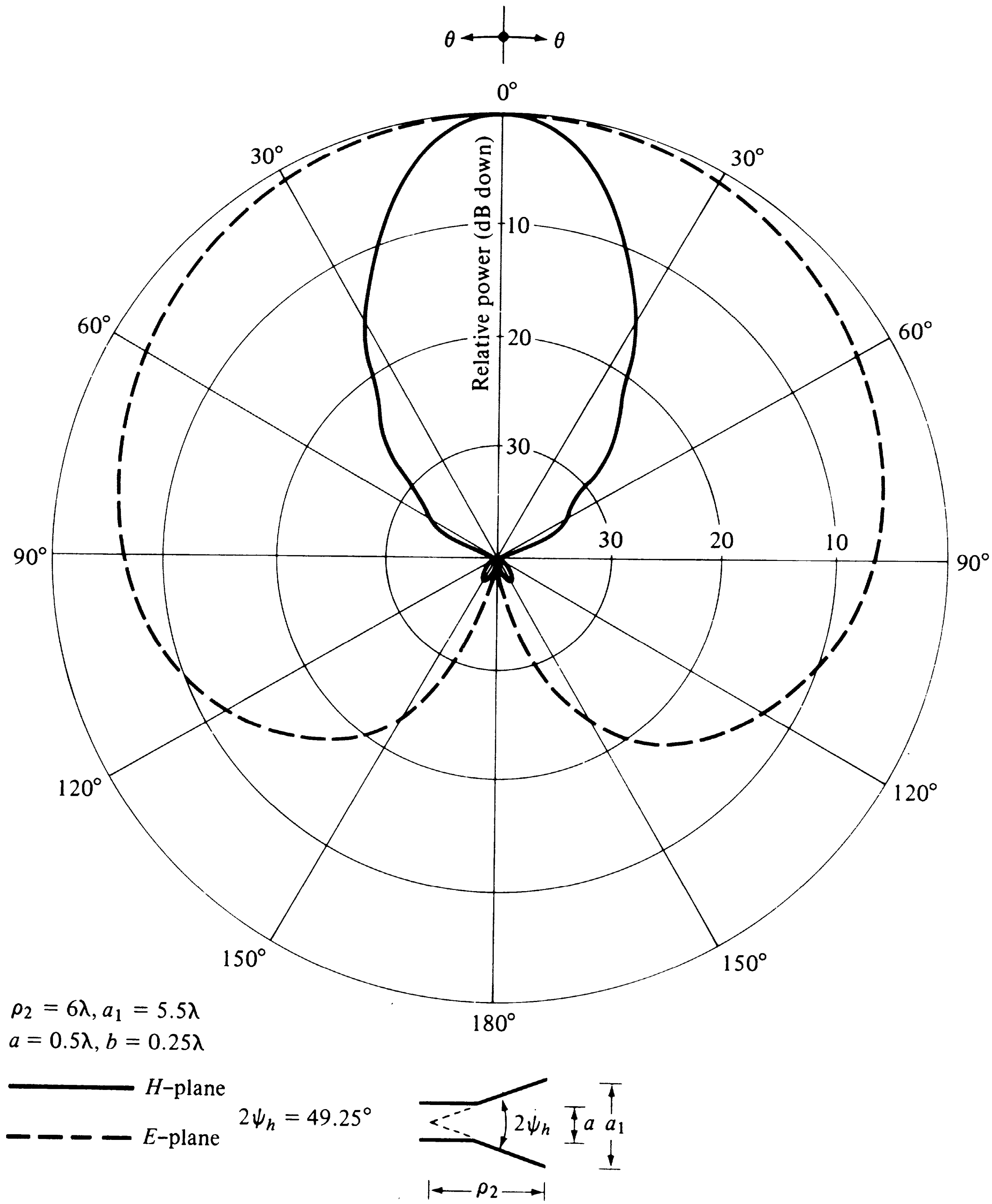

Fig. 13-12, Balanis, p. 674

The directivity of the H-plane sectoral horn is calculated by the general directivity expression for apertures (for derivation, see Lecture 17):

$$D_0 = \frac{4\pi}{\lambda^2} \cdot \frac{\left| \iint_{S_A} \mathbf{E}_a ds' \right|^2}{\iint_{S_A} |\mathbf{E}_a|^2 ds'}. \quad (18.21)$$

The integral in the denominator is proportional to the total radiated power,

$$2\eta\Pi_{rad} = \iint_{S_A} |\mathbf{E}_a|^2 ds' = \int_{-b/2}^{+b/2} \int_{-A/2}^{+A/2} |E_0|^2 \cos^2\left(\frac{\pi}{A}x'\right) dx'dy' = |E_0|^2 \frac{Ab}{2}. \quad (18.22)$$

In the solution of the integral in the numerator of (18.21), the field is substituted with its phase approximated as in (18.8). The final result is

$$D_H = \frac{b}{\lambda}\frac{32}{\pi}\left(\frac{A}{\lambda}\right)\varepsilon_{ph}^H = \frac{4\pi}{\lambda^2}\varepsilon_t \varepsilon_{ph}^H (Ab), \quad (18.23)$$

where

$$\varepsilon_t = \frac{8}{\pi^2};$$

$$\varepsilon_{ph}^H = \frac{\pi^2}{64t}\left\{ \left[C(p_1) - C(p_2)\right]^2 + \left[S(p_1) - S(p_2)\right]^2 \right\};$$

$$p_1 = 2\sqrt{t}\left[1 + \frac{1}{8t}\right], \quad p_2 = 2\sqrt{t}\left[-1 + \frac{1}{8t}\right];$$

$$t = \frac{1}{8}\left(\frac{A}{\lambda}\right)^2 \frac{1}{R_0/\lambda}.$$

The factor ε_t explicitly shows the aperture efficiency associated with the aperture cosine taper. The factor ε_{ph}^H is the aperture efficiency associated with the aperture phase distribution.

A family of universal directivity curves is given below. From these curves, it is obvious that for a given axial length R_0 and at a given wavelength, there is an optimal aperture width A corresponding to the maximum directivity.

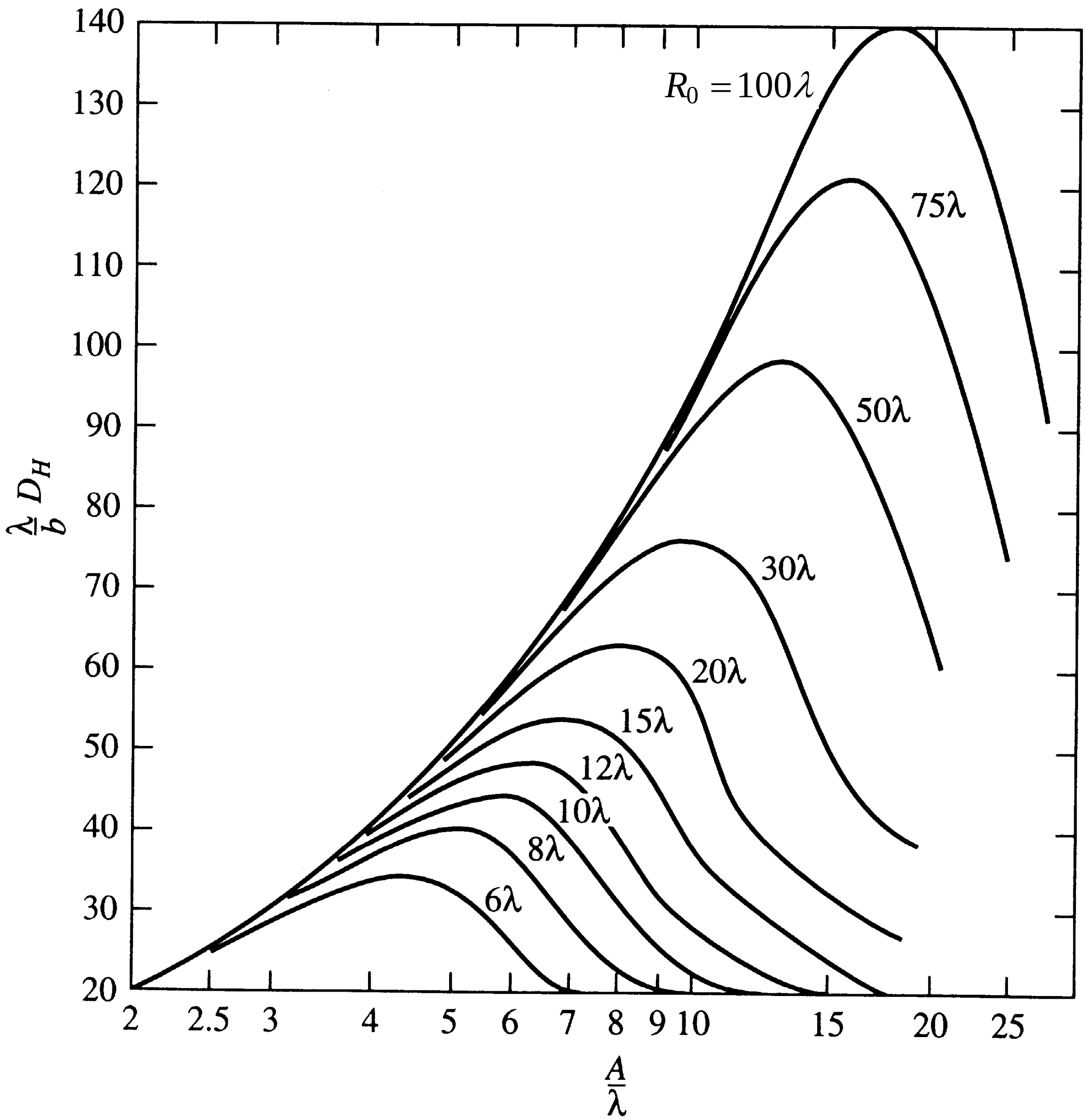

Stutzman

It can be shown that the optimal directivity is obtained if the relation between A and R_0 is

$$A = \sqrt{3\lambda R_0}\,, \tag{18.24}$$

or

$$\frac{A}{\lambda} = \sqrt{3\frac{R_0}{\lambda}}\,. \tag{18.25}$$

1.2 <u>The *E*-plane sectoral horn</u>

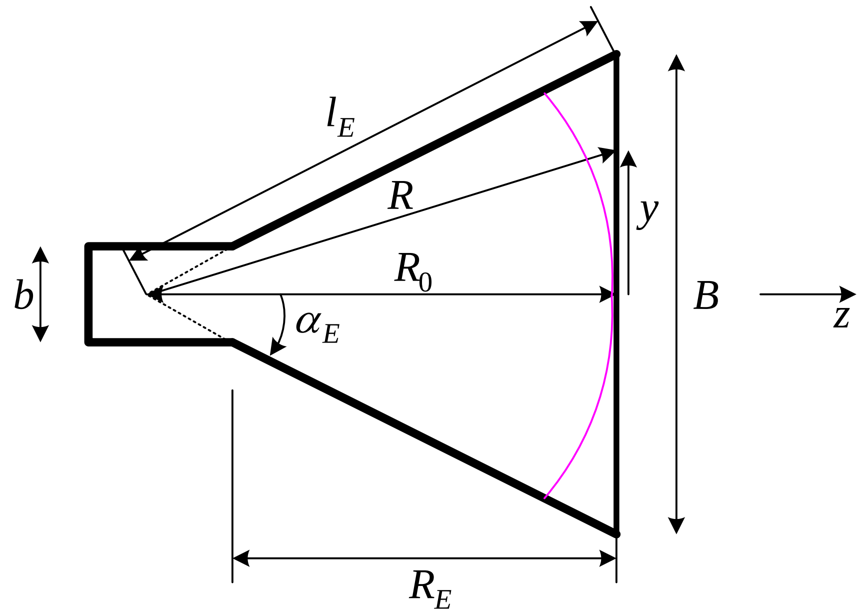

E-plane (*y*-*z*) cut of an *E*-plane sectoral horn

The geometry of the *E*-plane sectoral horn in the *E*-plane (*y*-*z* plane) is analogous to that of the *H*-plane sectoral horn in the *H*-plane. The analysis is following the same lines as in the previous section. The field at the aperture is approximated by [compare with (18.8)]

$$E_{a_y} = E_0 \cos\left(\frac{\pi}{a}x\right) e^{-j\frac{\beta}{2R_0}y^2} . \tag{18.26}$$

Here, the approximations

$$R = \sqrt{R_0^2 + y^2} = R_0\sqrt{1+\left(\frac{y}{R_0}\right)^2} \approx R_0\left[1+\frac{1}{2}\left(\frac{y}{R_0}\right)^2\right] \tag{18.27}$$

and

$$R - R_0 \approx \frac{1}{2}\frac{y^2}{R_0} \tag{18.28}$$

are made, which are analogous to (18.6) and (18.7).

The radiation field is obtained as

$$\mathbf{E} = j\beta E_0 \frac{4a}{\pi}\sqrt{\frac{\pi R_0}{\beta}}\frac{e^{-j\beta r}}{4\pi r}e^{j\left(\frac{\beta R_0}{2}\right)\left(\frac{\beta B}{2}\sin\theta\sin\varphi\right)^2}\cdot\left(\hat{\boldsymbol{\theta}}\sin\varphi+\hat{\boldsymbol{\varphi}}\cos\varphi\right)$$

$$\times\frac{(1+\cos\theta)}{2}\frac{\cos\left(\frac{\beta a}{2}\sin\theta\cos\varphi\right)}{\left[1-\left(\frac{\beta a}{2}\sin\theta\cos\varphi\right)^2\right]}\left[C(r_2)-jS(r_2)-C(r_1)+jS(r_1)\right]. \tag{18.29}$$

The arguments of the Fresnel integrals used in (18.29) are

$$r_1 = \sqrt{\frac{\beta}{\pi R_0}}\left(-\frac{B}{2}-R_0\frac{\beta B}{2}\sin\theta\sin\varphi\right),$$
$$r_2 = \sqrt{\frac{\beta}{\pi R_0}}\left(+\frac{B}{2}-R_0\frac{\beta B}{2}\sin\theta\sin\varphi\right). \tag{18.30}$$

Principal-plane patterns

The **normalized *H*-plane pattern** is found by substituting $\varphi = 0$ in (18.29):

$$\bar{H}(\theta) = \left(\frac{1+\cos\theta}{2}\right)\times\frac{\cos\left(\frac{\beta a}{2}\sin\theta\right)}{1-\left(\frac{\beta a}{2}\sin\theta\right)^2}. \tag{18.31}$$

The second factor in this expression is the pattern of a uniform-phase cosine-amplitude tapered line source. (Prove!)

The **normalized *E*-plane pattern** is found by substituting $\varphi = 90^\circ$ in (18.29):

$$\bar{E}(\theta) = \frac{1+\cos\theta}{2}\left|f_E(\theta)\right| = \frac{1+\cos\theta}{2}\sqrt{\frac{\left[C(r_2)-C(r_1)\right]^2+\left[S(r_2)-S(r_1)\right]^2}{4\left[C^2(r_{\theta=0})+S^2(r_{\theta=0})\right]}}. \tag{18.32}$$

Here, the arguments of the Fresnel integrals are calculated for $\varphi = 90^\circ$:

$$r_1 = \sqrt{\frac{\beta}{\pi R_0}}\left(-\frac{B}{2} - R_0\frac{\beta B}{2}\sin\theta\right),$$
$$r_2 = \sqrt{\frac{\beta}{\pi R_0}}\left(+\frac{B}{2} - R_0\frac{\beta B}{2}\sin\theta\right), \quad (18.33)$$

and

$$r_{\theta=0} = r_2(\theta = 0) = \frac{B}{2}\sqrt{\frac{\beta}{\pi R_0}}\,. \quad (18.34)$$

Similar to the *H*-plane sectoral horn, the principal *E*-plane pattern can be accurately calculated if no approximation of the phase distribution is made. Then, the function $f_E(\theta)$ has to be calculated by numerical integration of (compare with (18.20))

$$f_E(\theta) \propto \int_{-B/2}^{B/2} e^{-j\beta\sqrt{R_0^2 + y'^2}} e^{j\beta \sin\theta \cdot y'} dy'\,. \quad (18.35)$$

E- AND *H*-PLANE PATTERN OF *E*-PLANE SECTORAL HORN

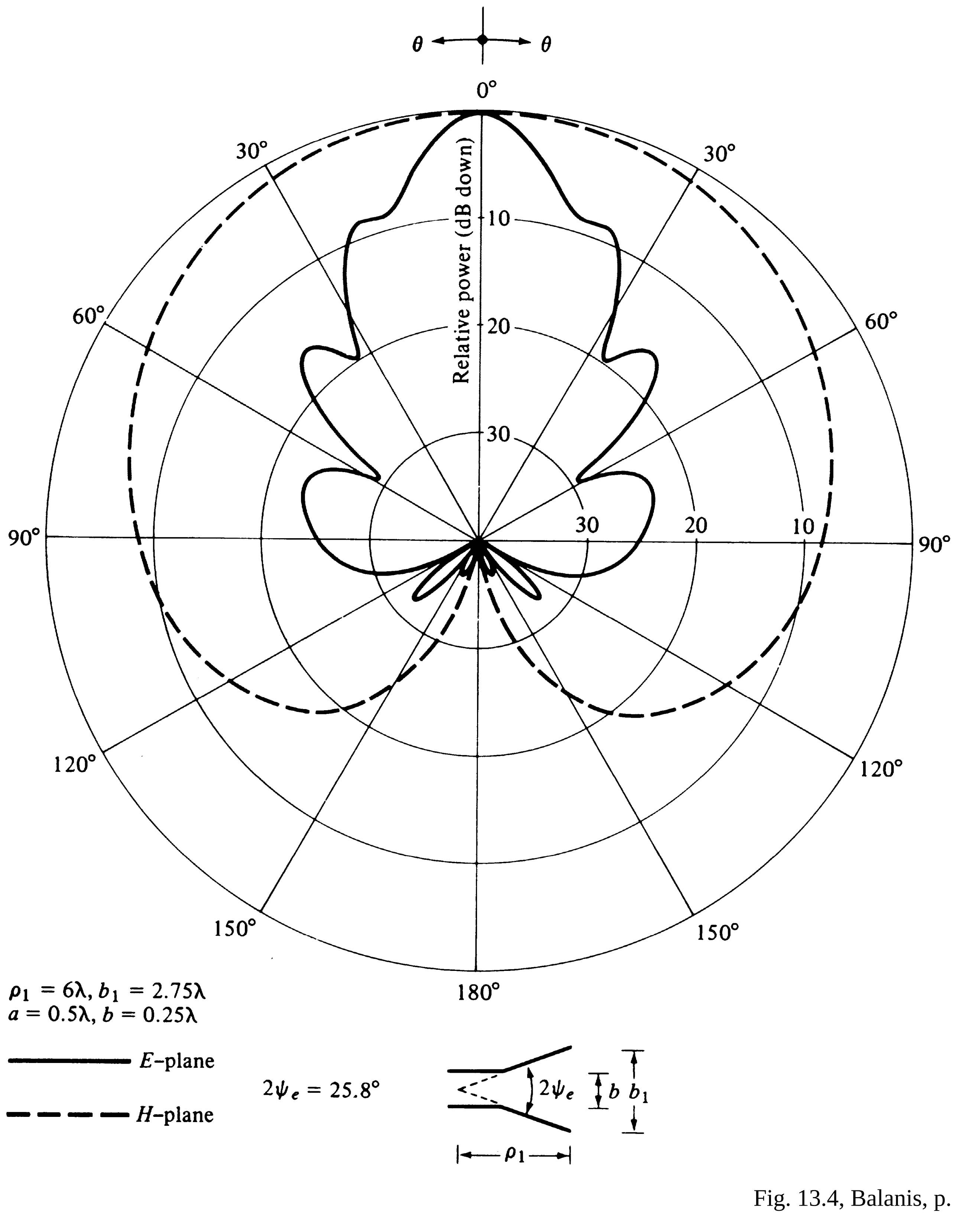

Fig. 13.4, Balanis, p. 660

Directivity

The directivity of the E-plane sectoral horn is found in a manner analogous to the H-plane sectoral horn:

$$D_E = \frac{a}{\lambda}\frac{32}{\pi}\frac{B}{\lambda}\varepsilon_{ph}^{E} = \frac{4\pi}{\lambda^2}\varepsilon_t\varepsilon_{ph}^{E} aB, \qquad (18.36)$$

where

$$\varepsilon_t = \frac{8}{\pi^2},\ \varepsilon_{ph}^{E} = \frac{C^2(q)+S^2(q)}{q^2},\ \ q = \frac{B}{\sqrt{2\lambda R_0}}.$$

A family of universal directivity curves $\lambda D_E / a$ vs. B/λ with R_0 being a parameter is given below.

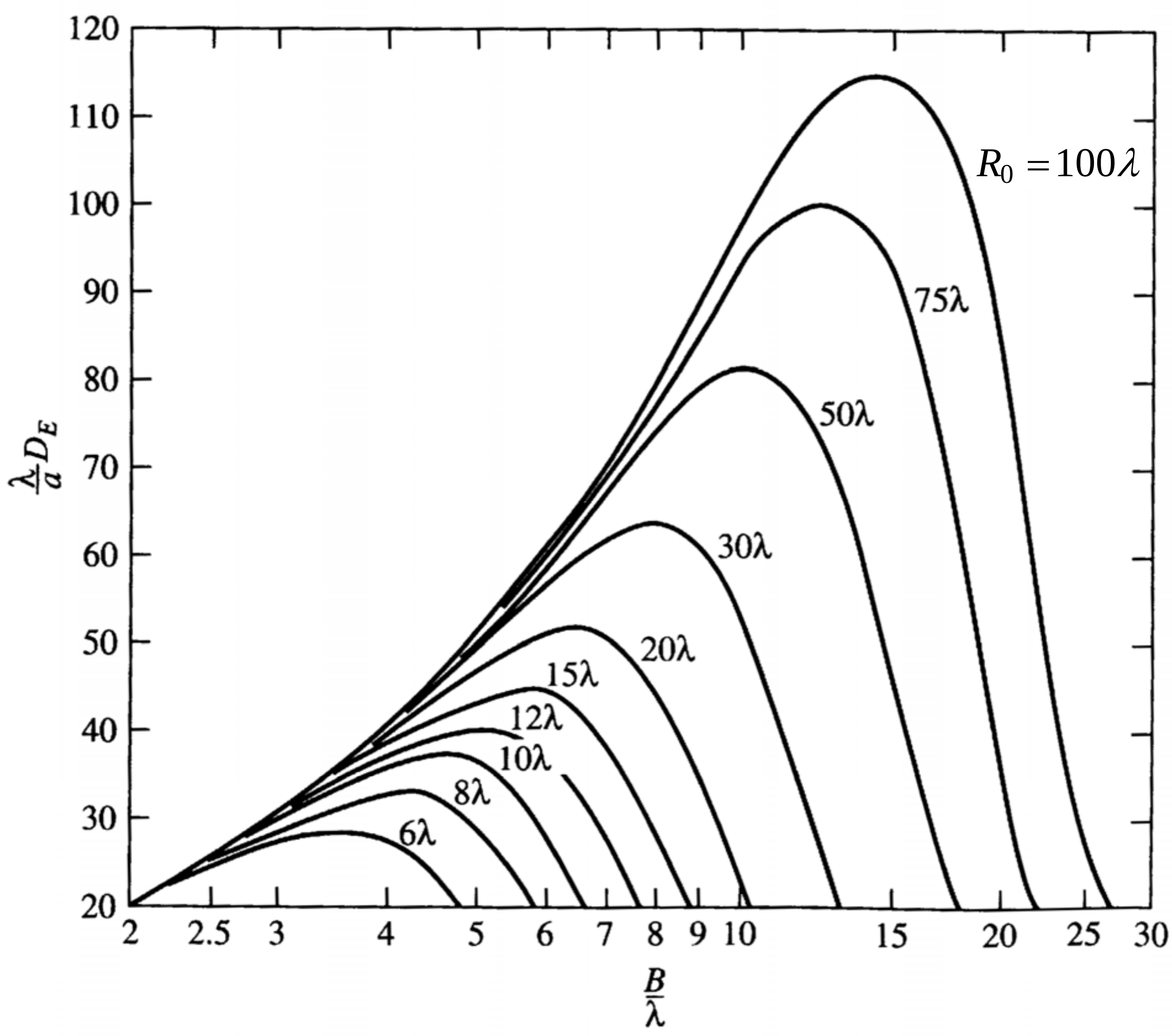

The optimal relation between the flared height B and the horn length R_0 is

$$B = \sqrt{2\lambda R_0}\,. \tag{18.37}$$

1.3 The pyramidal horn

The pyramidal horn is probably the most popular antenna in the microwave frequency ranges (from ≈ 1 GHz up to ≈ 18 GHz). The feeding waveguide is flared in both directions, the E-plane and the H-plane. All results are combinations of the E-plane sectoral horn and the H-plane sectoral horn analyses. The field distribution at the aperture is approximated as

$$E_{a_y} = E_0 \cos\left(\frac{\pi}{A}x\right) e^{-j\frac{\beta}{2}\left(\frac{x^2}{R_0^{E2}} + \frac{y^2}{R_0^{H2}}\right)}. \tag{18.38}$$

The E-plane principal pattern of the pyramidal horn is the same as the E-plane principal pattern of the E-plane sectoral horn. The same holds for the H-plane patterns of the pyramidal horn and the H-plane sectoral horn.

The directivity of the pyramidal horn can be found by introducing the phase efficiency factors of both planes and the taper efficiency factor of the H-plane:

$$D_P = \frac{4\pi}{\lambda^2}\varepsilon_t \varepsilon_{ph}^{E} \varepsilon_{ph}^{H} (AB), \tag{18.39}$$

where

$$\varepsilon_t = \frac{8}{\pi^2};$$

$$\varepsilon_{ph}^{H} = \frac{\pi^2}{64t}\left\{\left[C(p_1) - C(p_2)\right]^2 + \left[S(p_1) - S(p_2)\right]^2\right\};$$

$$p_1 = 2\sqrt{t}\left[1 + \frac{1}{8t}\right],\quad p_2 = 2\sqrt{t}\left[-1 + \frac{1}{8t}\right],\ t = \frac{1}{8}\left(\frac{A}{\lambda}\right)^2 \frac{1}{R_0^H / \lambda};$$

$$\varepsilon_{ph}^{E} = \frac{C^2(q) + S^2(q)}{q^2},\quad q = \frac{B}{\sqrt{2\lambda R_0^E}}.$$

The gain of a horn is usually very close to its directivity because the radiation efficiency is very good (low losses). The directivity as calculated with (18.39) is very close to measurements. The above expression is a physical optics approximation, and it does not take into account only multiple diffractions, and the diffraction at the edges of the horn arising from reflections from the horn interior. These phenomena, which are unaccounted for, lead to minor fluctuations of the measured results about the prediction of (18.39). That is why horns are often used as ***gain standards*** in antenna measurements.

The optimal directivity of an *E*-plane horn is achieved at $q=1$ [see also (18.37)], $\varepsilon_{ph}^{E}=0.8$. The optimal directivity of an *H*-plane horn is achieved at $t=3/8$ [see also (18.24)], $\varepsilon_{ph}^{H}=0.79$. Thus, the optimal horn has a phase aperture efficiency of

$$\varepsilon_{ph}^{P}=\varepsilon_{ph}^{H}\varepsilon_{ph}^{E}=0.632. \qquad (18.40)$$

The total aperture efficiency includes the taper factor, too:

$$\varepsilon_{ph}^{P}=\varepsilon_{t}\varepsilon_{ph}^{H}\varepsilon_{ph}^{E}=0.81\cdot 0.632=0.51. \qquad (18.41)$$

Therefore, the best achievable directivity for a rectangular waveguide horn is about half that of a uniform rectangular aperture.

We reiterate that best accuracy is achieved if ε_{ph}^{H} and ε_{ph}^{E} are calculated numerically without using the second-order phase approximations in (18.7) and (18.28).

Optimum horn design

Usually, the optimum (from the point of view of maximum gain) design of a horn is desired because it results in the shortest axial length. The whole design can be actually reduced to the solution of a single fourth-order equation. For a horn to be realizable, the following must be true:

$$R_E=R_H=R_P. \qquad (18.42)$$

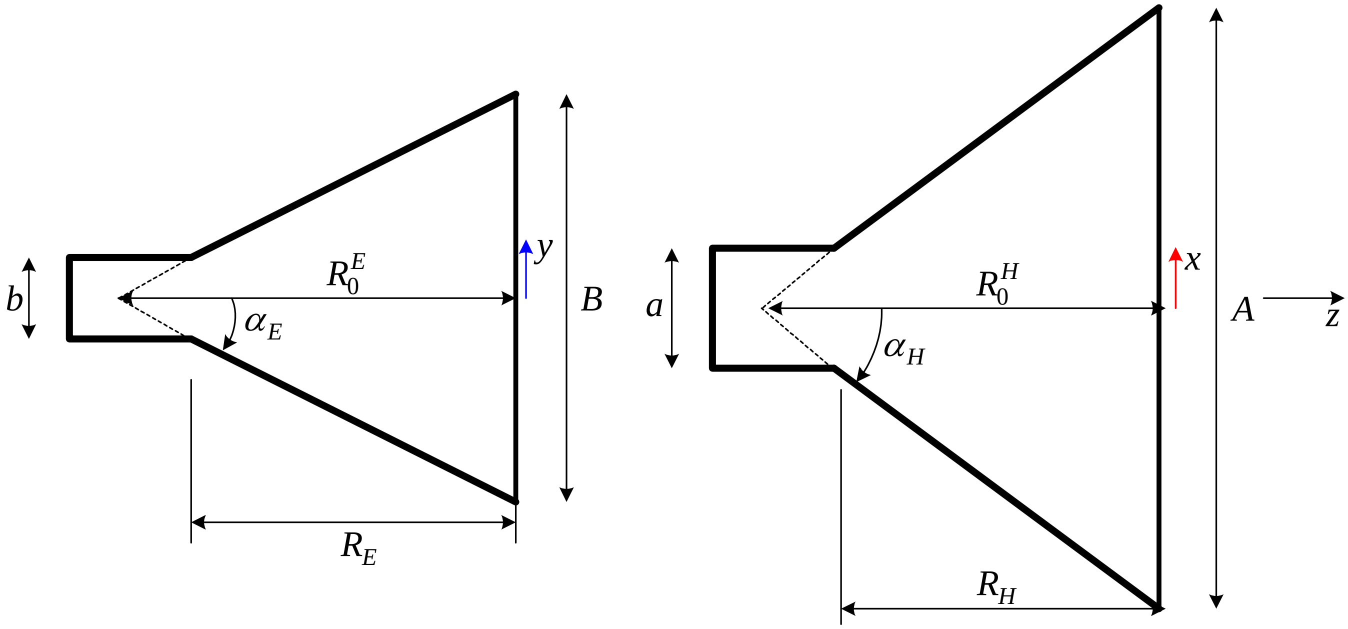

It can be shown that

$$\frac{R_0^H}{R_H} = \frac{A/2}{A/2 - a/2} = \frac{A}{A-a}, \tag{18.43}$$

$$\frac{R_0^E}{R_E} = \frac{B/2}{B/2 - b/2} = \frac{B}{B-b}. \tag{18.44}$$

The optimum-gain condition in the *E*-plane (18.37) is substituted in (18.44) to produce

$$B^2 - bB - 2\lambda R_E = 0. \tag{18.45}$$

There is only one physically meaningful solution to (18.45):

$$B = \frac{1}{2}\left(b + \sqrt{b^2 + 8\lambda R_E}\right). \tag{18.46}$$

Similarly, the maximum-gain condition for the *H*-plane of (18.24) together with (18.43) yields

$$R_H = \frac{A-a}{A}\left(\frac{A^2}{3\lambda}\right) = A\frac{(A-a)}{3\lambda}. \tag{18.47}$$

Since $R_E = R_H$ must be fulfilled, (18.47) is substituted in (18.46), which gives

$$B = \frac{1}{2}\left(b + \sqrt{b^2 + \frac{8A(A-a)}{3}} \right). \qquad (18.48)$$

Substituting in the expression for the horn's gain

$$G = \frac{4\pi}{\lambda^2} \varepsilon_{ap} AB, \qquad (18.49)$$

gives the relation between A, the gain G, and the aperture efficiency ε_{ap}:

$$G = \frac{4\pi}{\lambda^2} \varepsilon_{ap} A \frac{1}{2}\left(b + \sqrt{b^2 + \frac{8A(a-a)}{3}} \right), \qquad (18.50)$$

$$\Rightarrow A^4 - aA^3 + \frac{3bG\lambda^2}{8\pi\varepsilon_{ap}} A - \frac{3G^2\lambda^4}{32\pi^2\varepsilon_{ap}^2} = 0. \qquad (18.51)$$

Equation (18.51) is the optimum pyramidal horn design equation. The optimum-gain value of $\varepsilon_{ap} = 0.51$ is usually used, which makes the equation a fourth-order polynomial equation in A. Its roots can be found analytically (which is not particularly easy) and numerically. In a numerical solution, the first guess is usually set at $A^{(0)} = 0.45\lambda\sqrt{G}$. Once A is found, B can be computed from (18.48) and $R_E = R_H$ is computed from (18.47).

Sometimes, an optimal horn is desired for a given axial length R_0. In this case, there is no need for nonlinear-equation solution. The design procedure follows the steps: (a) find A from (18.24), (b) find B from (18.37), and (c) calculate the gain G using (18.49) where $\varepsilon_{ap} = 0.51$.

Horn antennas operate well over a bandwidth of 50 %. However, gain performance is optimal only at a given frequency. To understand better the frequency dependence of the directivity and the aperture efficiency, the plot of these curves for an X-band (8.2 GHz to 12.4 GHz) horn fed by WR90 waveguide is given below ($a = 0.9$ in. = 2.286 cm and $b = 0.4$ in. = 1.016 cm).

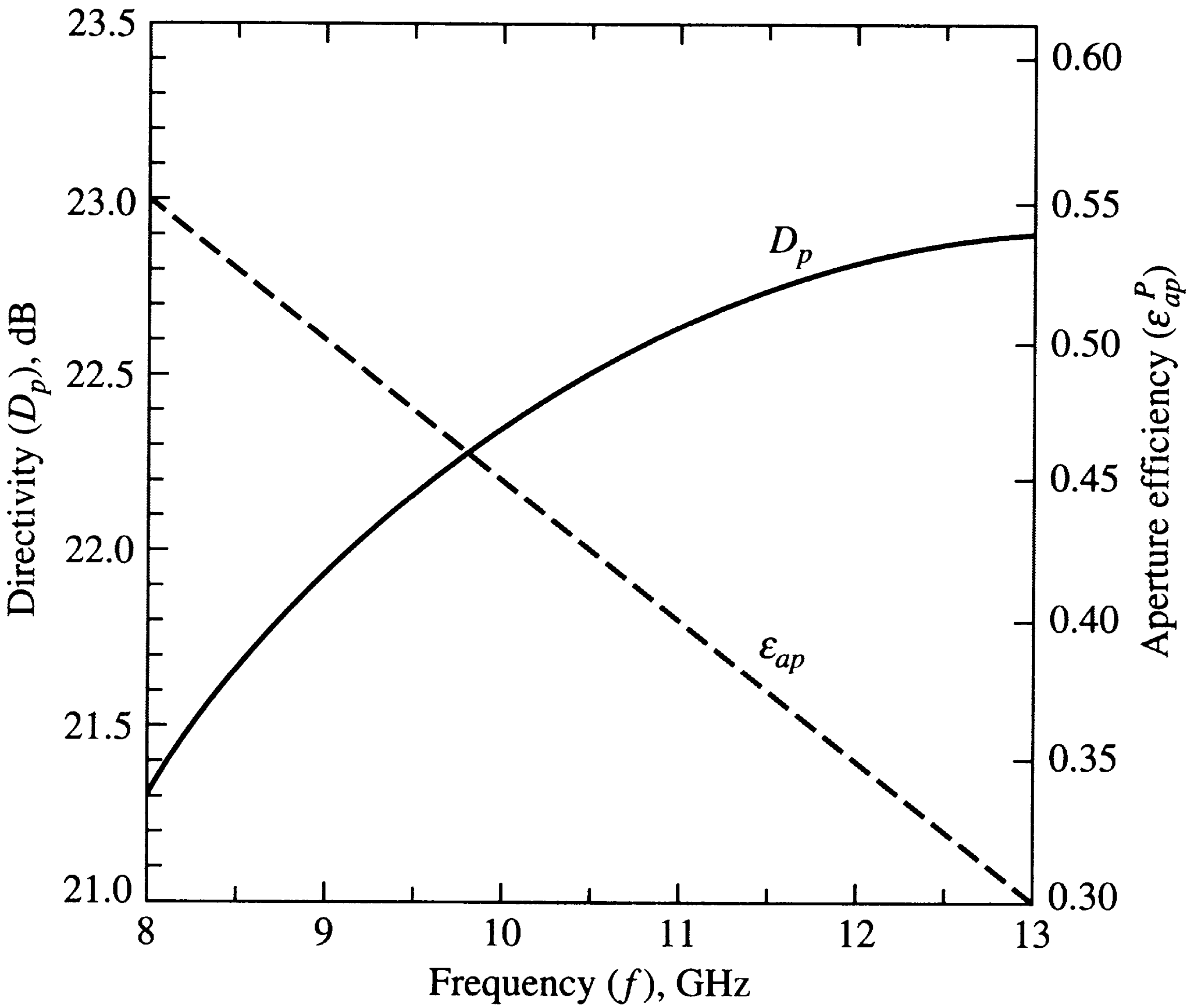

The gain increases with frequency, which is typical for aperture antennas. However, the curve shows saturation at higher frequencies. This is due to the decrease of the aperture efficiency, which is a result of an increased phase difference in the field distribution at the aperture.

The pattern of a “large” pyramidal horn ($f = 10.525$ GHz, feeder is waveguide WR90):

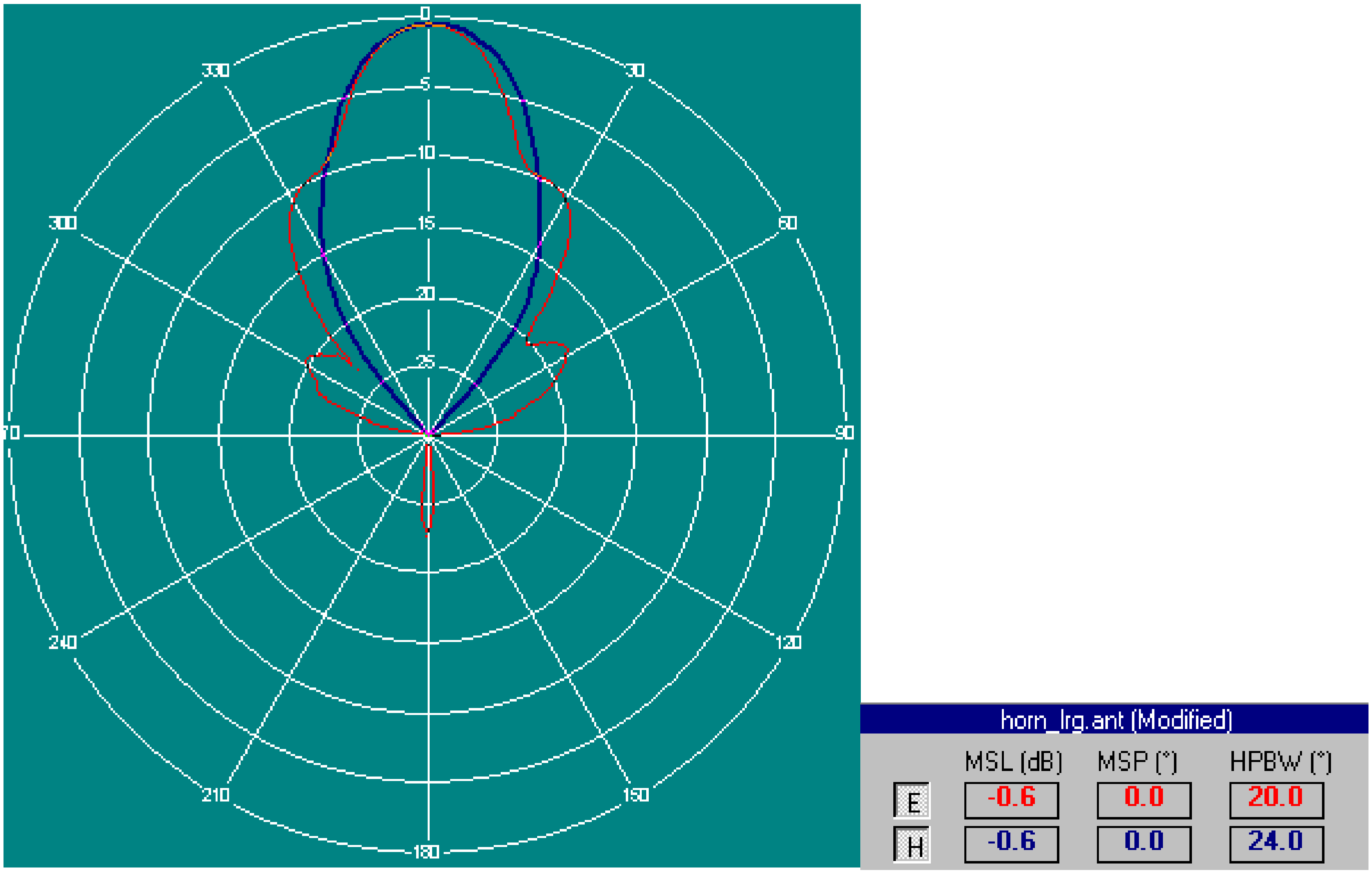

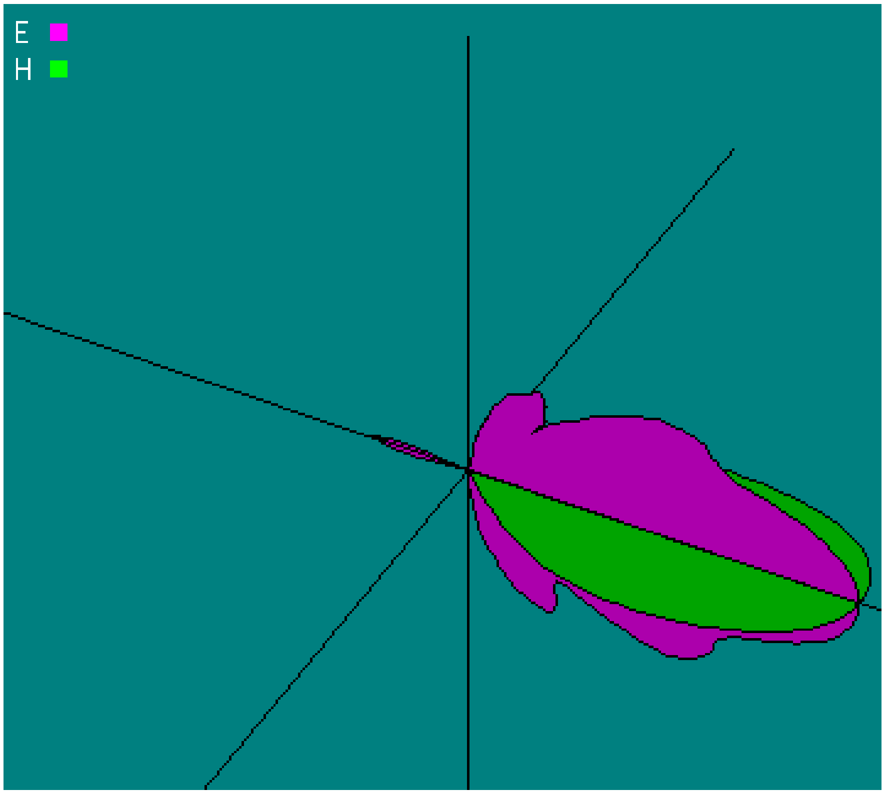

Comparison of the *E*-plane patterns of a waveguide open end, “small” pyramidal horn and “large” pyramidal horn:

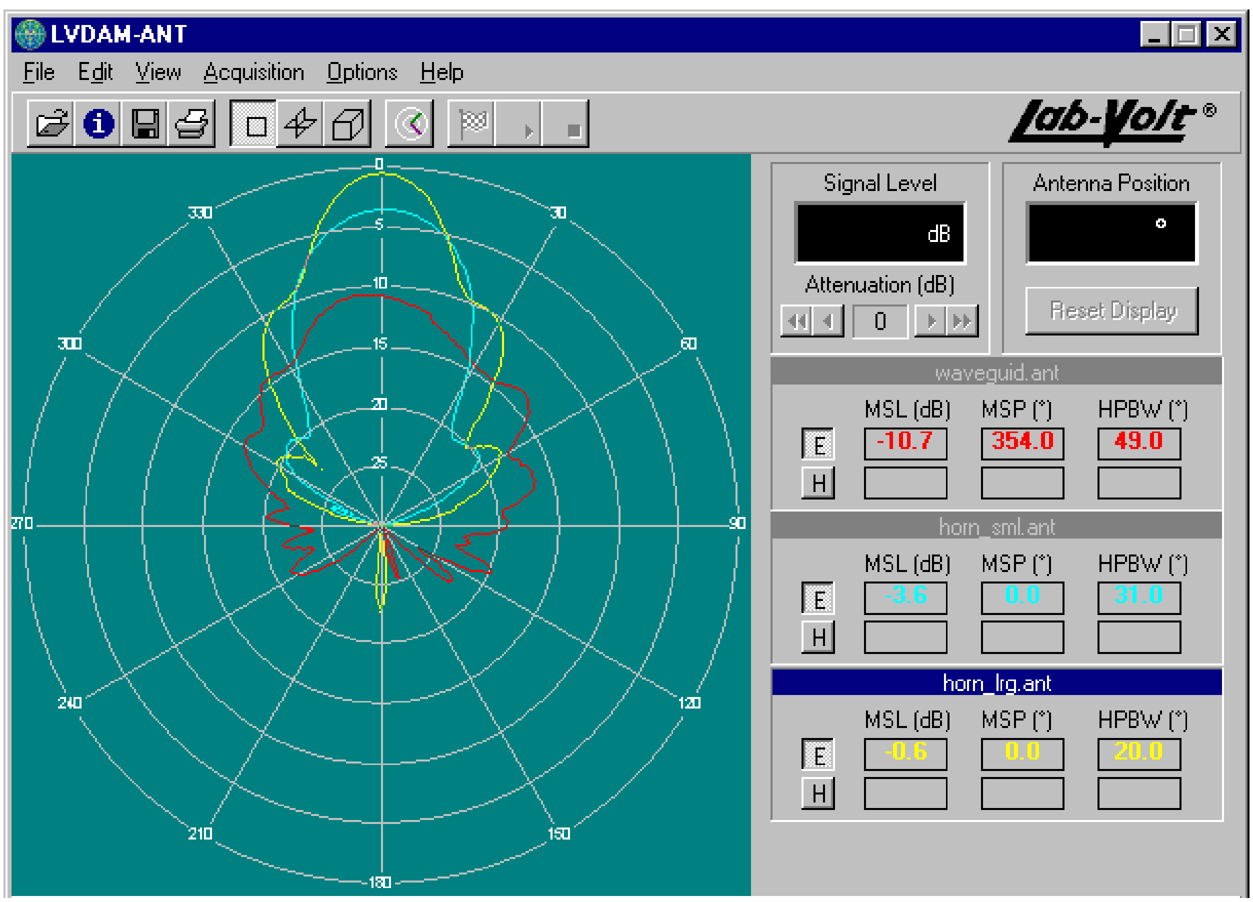

Note the multiple side lobes and the significant back lobe. They are due to diffraction at the horn edges, which are perpendicular to the **E** field. To reduce edge diffraction, enhancements are proposed for horn antennas such as

- corrugated horns
- aperture-matched horns

Corrugated horns taper the **E** field in the vertical direction, thus, reducing side-lobes and diffraction from edges. The overall main beam becomes smooth and nearly rotationally symmetrical (esp. for $A \approx B$). This is important when the horn is used as a feed to a reflector antenna.

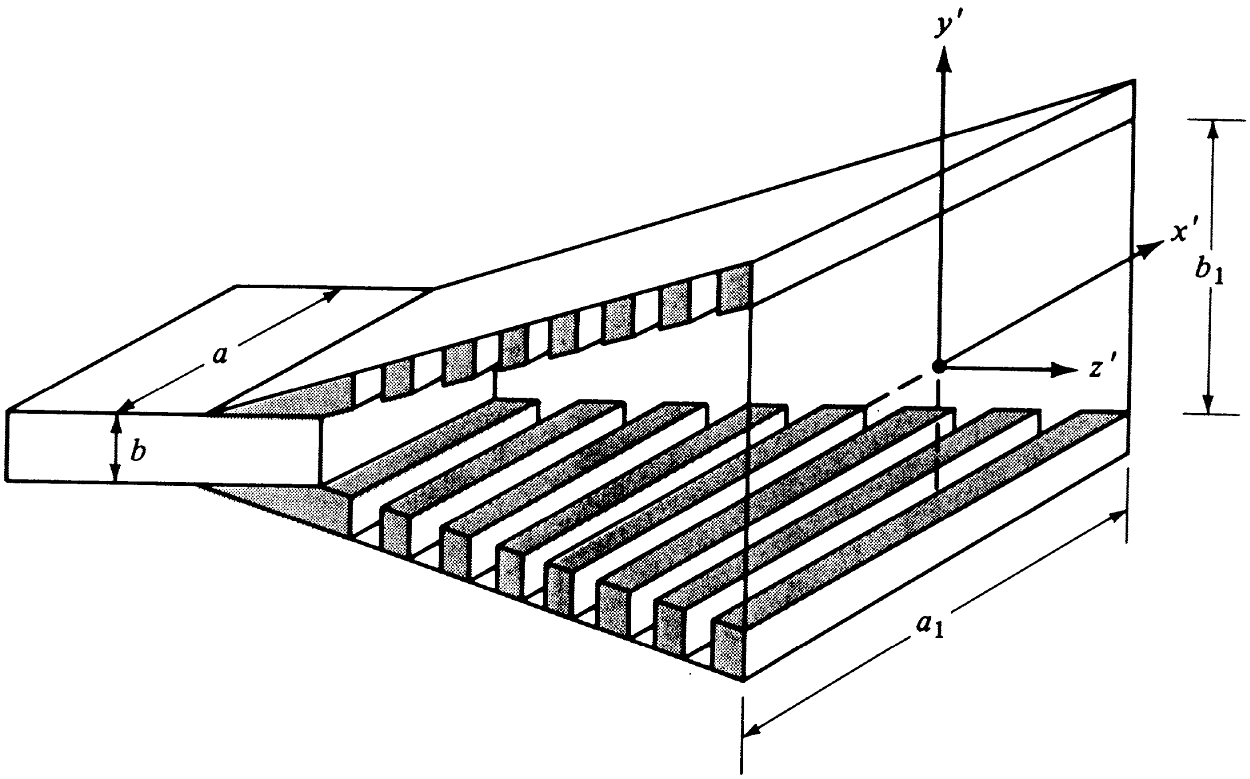

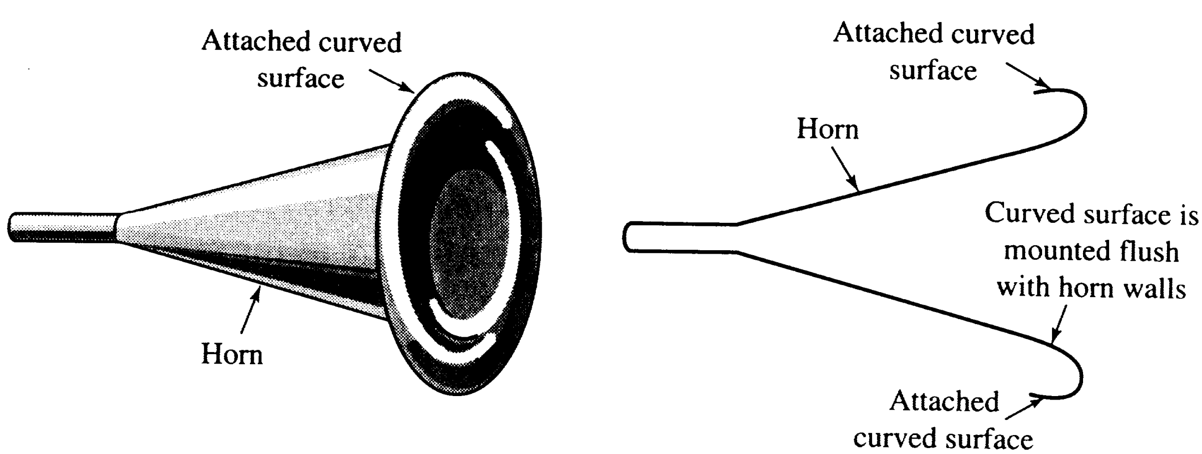

Comparison of the *H*-plane patterns of a waveguide open end, “small” pyramidal horn and “large” pyramidal horn:

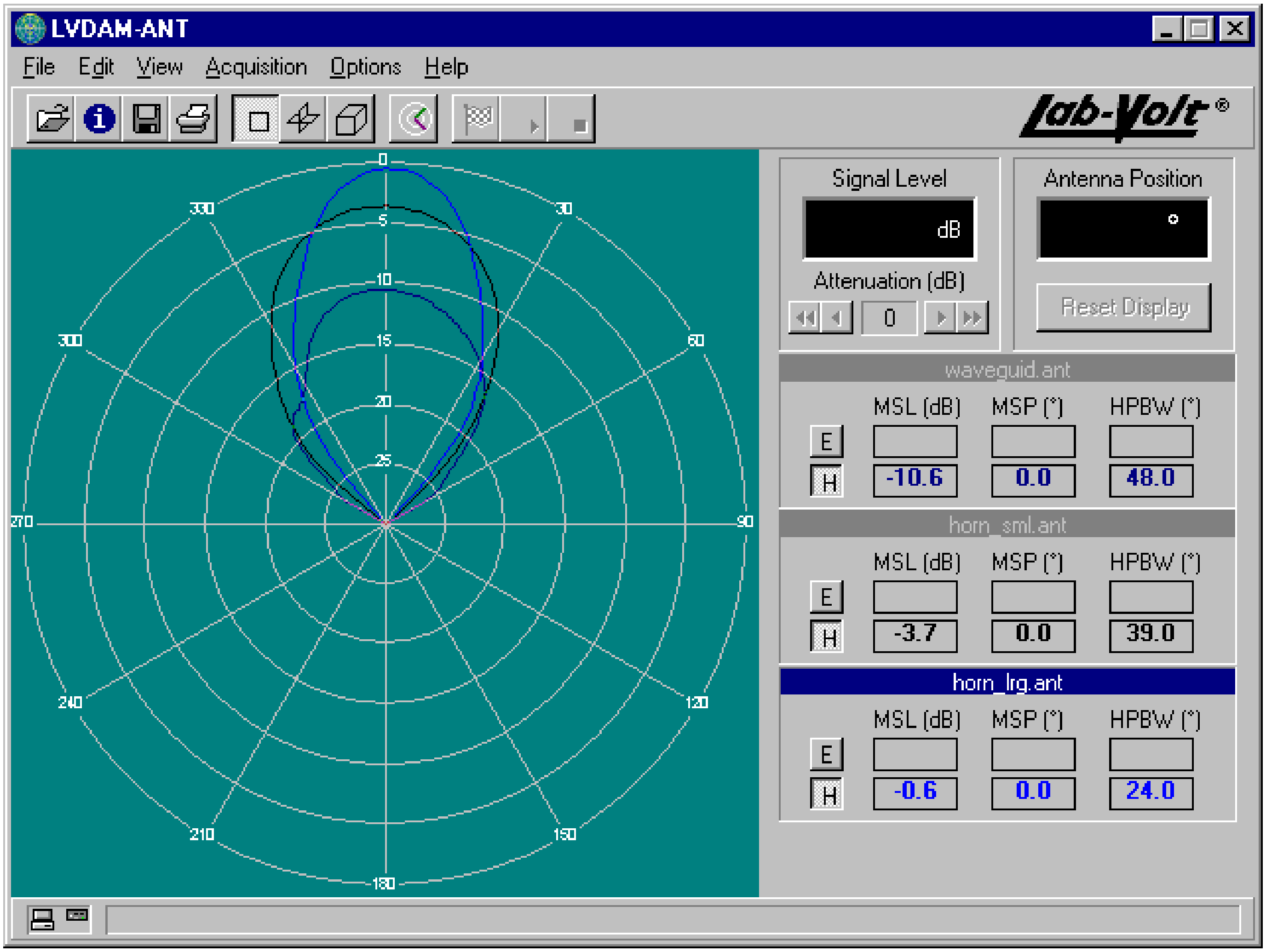

2 Circular apertures

2.1 A uniform circular aperture

The uniform circular aperture is approximated by a circular opening in a ground plane illuminated by a uniform plane wave normally incident from behind.

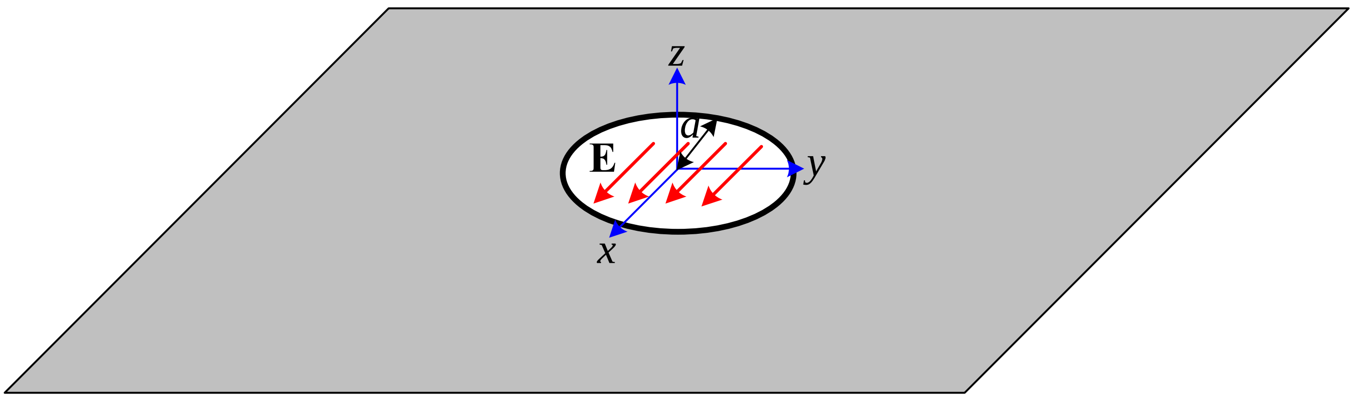

The field distribution is described as

$$\mathbf{E}_a = \hat{\mathbf{x}} E_0, \quad \rho' \le a. \tag{18.52}$$

The radiation integral is

$$I_x^E = E_0 \iint_{S_a} e^{j\beta \hat{\mathbf{r}}\cdot\mathbf{r}'} ds'. \tag{18.53}$$

The integration point is at

$$\mathbf{r}' = \hat{\mathbf{x}}\rho'\cos\varphi' + \hat{\mathbf{y}}\rho'\sin\varphi'. \tag{18.54}$$

In (18.54), cylindrical coordinates are used, therefore,

$$\hat{\mathbf{r}}\cdot\mathbf{r}' = \rho'\sin\theta(\cos\varphi\cos\varphi' + \sin\varphi\sin\varphi') = \rho'\sin\theta\cos(\varphi-\varphi'). \tag{18.55}$$

Hence, (18.53) becomes

$$I_x^E = E_0 \int_0^a \left[\int_0^{2\pi} e^{j\beta\rho'\sin\theta\cos(\varphi-\varphi')} d\varphi' \right] \rho' d\rho' = 2\pi E_0 \int_0^a \rho' J_0(\beta\rho'\sin\theta) d\rho'. \tag{18.56}$$

Here, J_0 is the Bessel function of the first kind of order zero. Applying the identity

$$\int xJ_0(x)dx = xJ_1(x) \tag{18.57}$$

to (18.56) leads to

$$I_x^E = 2\pi E_0 \frac{a}{\beta \sin\theta} J_1(\beta a \sin\theta). \tag{18.58}$$

In this case, the equivalent magnetic current formulation of the equivalence principle is used [see Lecture 17]. The far field is obtained as

$$\begin{aligned}\mathbf{E} &= \left(\hat{\boldsymbol{\theta}}\cos\varphi - \hat{\boldsymbol{\varphi}}\cos\theta\sin\varphi\right) j\beta \frac{e^{j\beta r}}{2\pi r} I_x^E = \\ &= \left(\hat{\boldsymbol{\theta}}\cos\varphi - \hat{\boldsymbol{\varphi}}\cos\theta\sin\varphi\right) j\beta E_0 \pi a^2 \frac{e^{j\beta r}}{2\pi r} \frac{2J_1(\beta a \sin\theta)}{\beta a \sin\theta}.\end{aligned} \tag{18.59}$$

<u>Principal-plane patterns</u>

***E*-plane** ($\varphi = 0$): $E_\theta(\theta) = \dfrac{2J_1(\beta a \sin\theta)}{\beta a \sin\theta}$ (18.60)

***H*-plane** ($\varphi = 90^\circ$): $E_\varphi(\theta) = \cos\theta \cdot \dfrac{2J_1(\beta a \sin\theta)}{\beta a \sin\theta}$ (18.61)

The 3-D amplitude pattern:

$$\bar{E}(\theta,\varphi) = \sqrt{1-\sin^2\theta\sin^2\varphi} \cdot \underbrace{\frac{2J_1(\beta a \sin\theta)}{\beta a \sin\theta}}_{f(\theta)} \tag{18.62}$$

The larger the aperture, the less significant the $\cos\theta$ factor is in (18.61) because the main beam in the $\theta = 0$ direction is very narrow and in this small solid angle $\cos\theta \approx 1$. Thus, the 3-D pattern of a large circular aperture features a fairly symmetrical beam.

Example plot of the principal-plane patterns for $a = 3\lambda$:

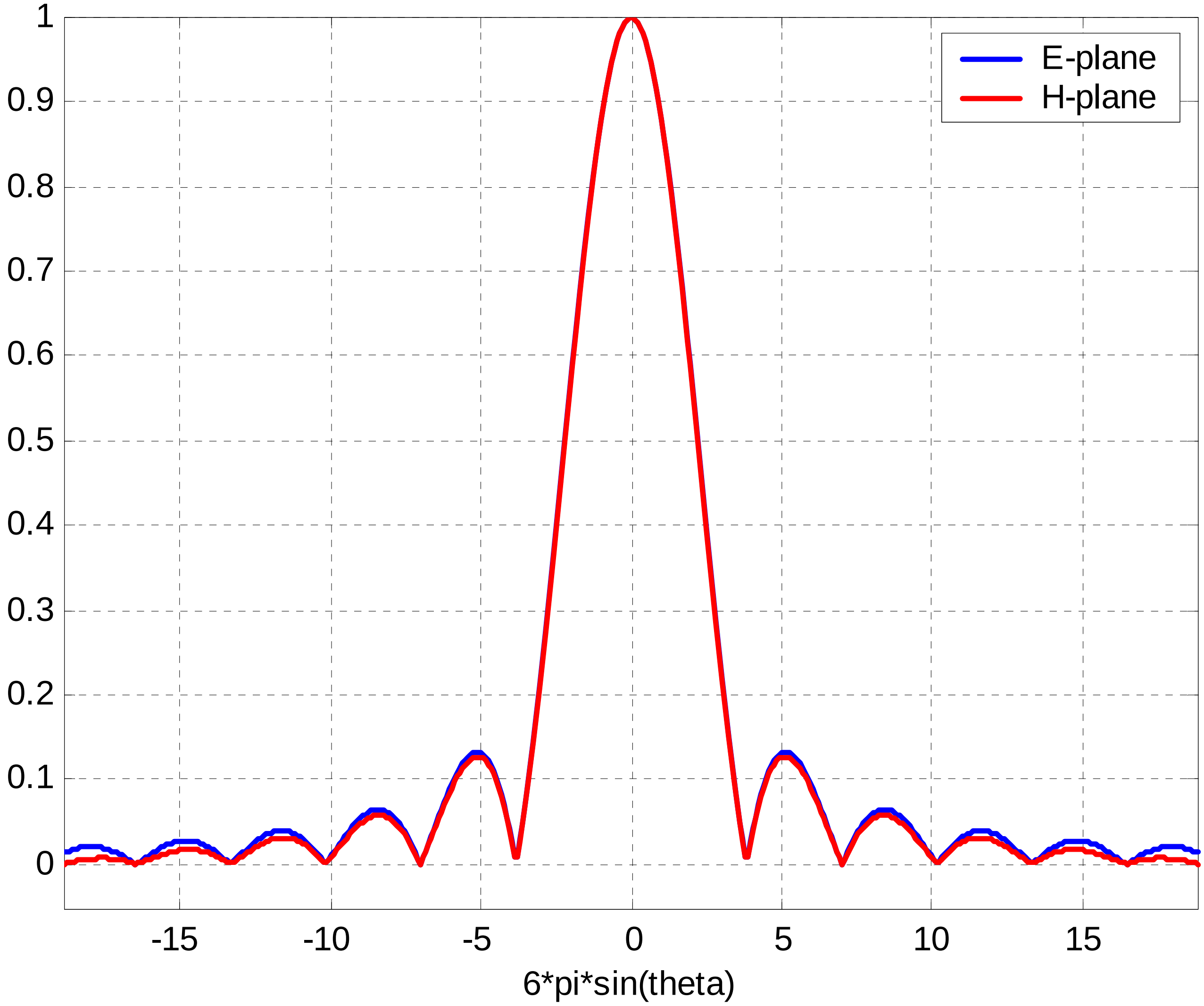

The half-power angle for the $f(\theta)$ factor is obtained at $\beta a \sin\theta = 1.6$. So, the HPBW for large apertures ($a \gg \lambda$) is given by

$$HPBW = 2\theta_{1/2} \simeq 2\arcsin\left(\frac{1.6}{\beta a}\right) \approx 2\frac{1.6}{\beta a} = 58.4\frac{\lambda}{2a}, \text{ deg.} \tag{18.63}$$

For example, if the diameter of the aperture is $2a = 10\lambda$, then $HPBW = 5.84°$.

The side-lobe level of any uniform circular aperture is 0.1332 (-17.5 dB).

Any uniform aperture has unity taper aperture efficiency, and its directivity can be found directly in terms of its physical area,

$$D_u = \frac{4\pi}{\lambda^2} A_p = \frac{4\pi}{\lambda^2}\pi a^2. \tag{18.64}$$

2.2 Tapered circular apertures

Many practical circular aperture antennas can be approximated as radially symmetric apertures with field amplitude distribution, which is tapered from the center toward the aperture edge. Then, the radiation integral (18.56) has a more general form:

$$I_x^E = 2\pi \int_0^a E_0(\rho')\rho' J_0(\beta\rho'\sin\theta) d\rho' . \tag{18.65}$$

In (18.65), we still assume that the field has axial symmetry, i.e., it does not depend on φ'. Often used approximation is the parabolic taper of order *n*:

$$E_a(\rho') = E_0 \left[1 - \left(\frac{\rho'}{a} \right)^2 \right]^n \tag{18.66}$$

where E_0 is a constant. This is substituted in (18.65) to calculate the respective component of the radiation integral:

$$I_x^E(\theta) = 2\pi E_0 \int_0^a \left[1 - \left(\frac{\rho'}{a} \right)^2 \right]^n \rho' J_0(\beta\rho'\sin\theta) d\rho' . \tag{18.67}$$

The following relation is used to solve (18.67):

$$\int_0^1 (1-x^2)^n x J_0(bx) dx = \frac{2^n n!}{b^{n+1}} J_{n+1}(b) . \tag{18.68}$$

In our case, $x = \rho'/a$ and $b = \beta a \sin\theta$. Then, $I_x^E(\theta)$ reduces to

$$I_x^E(\theta) = E_0 \frac{\pi a^2}{n+1} f(\theta, n) , \tag{18.69}$$

where

$$f(\theta, n) = \frac{2^{n+1}(n+1)! J_{n+1}(\beta a \sin\theta)}{\left(\beta a \sin\theta\right)^{n+1}} \tag{18.70}$$

is the normalized pattern (neglecting the angular factors such as $\cos\varphi$ and $\cos\theta\sin\varphi$).

The aperture taper efficiency is calculated to be

$$\varepsilon_t = \frac{\left[C + \frac{1-C}{n+1}\right]^2}{C^2 + \frac{2C(1-C)}{n+1} + \frac{(1-C)^2}{2n+1}}. \tag{18.71}$$

Here, C denotes the *pedestal height*. The pedestal height is the edge field illumination relative to the illumination at the center.

The properties of several common tapers are given in the tables below. The parabolic taper ($n=1$) provides lower side lobes in comparison with the uniform distribution ($n=0$) but it has a broader main beam. There is always a trade-off between low side-lobe levels and high directivity (small HPBW). More or less optimal solution is provided by the parabolic-on-pedestal aperture distribution. Moreover, this distribution approximates very closely the real case of circular reflector antennas, where the feed antenna pattern is intercepted by the reflector only out to the reflector rim.

a. Parabolic taper

$$E_a(\rho') = \left[1 - \left(\frac{\rho'}{a}\right)^2\right]^n$$

$$f(\theta, n) = \frac{2^{n+1}(n+1)!\,J_{n+1}(\beta a \sin\theta)}{(\beta a \sin\theta)^{n+1}}$$

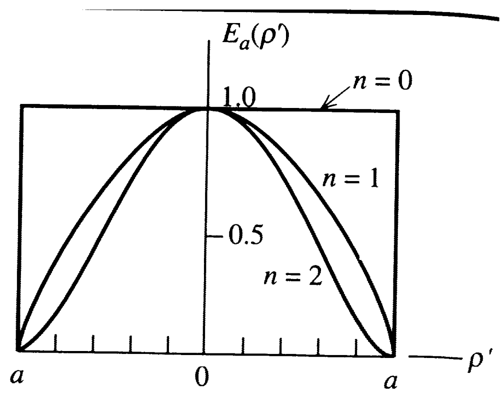

n	HP (rad)	Side Lobe Level (dB)	ε_t	Normalized Pattern $f(\theta, n)$	Distribution
0	$1.02\,\frac{\lambda}{2a}$	−17.6	1.00	$\frac{2J_1(\beta a \sin\theta)}{\beta a \sin\theta}$	Uniform
1	$1.27\,\frac{\lambda}{2a}$	−24.6	0.75	$\frac{8J_2(\beta a \sin\theta)}{(\beta a \sin\theta)^2}$	Parabolic
2	$1.47\,\frac{\lambda}{2a}$	−30.6	0.55	$\frac{48J_3(\beta a \sin\theta)}{(\beta a \sin\theta)^3}$	Parabolic squared

b. Parabolic taper on a pedestal

$$E_a(\rho') = C + (1 + C)\left[1 - \left(\frac{\rho'}{a}\right)^2\right]^n$$

$$f(\theta, n, C) = \frac{Cf(\theta, n = 0) + \dfrac{1 - C}{n + 1} f(\theta, n)}{C + \dfrac{1 - C}{n + 1}}$$

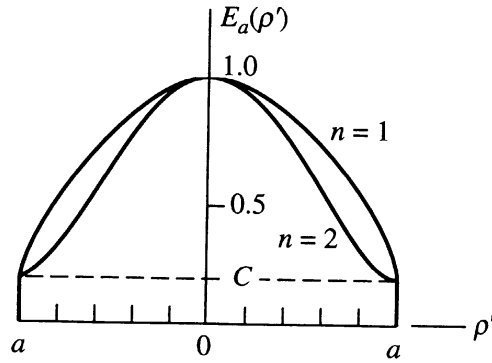

Edge Illumination		n = 1			n = 2		
C_{dB}	C	HP (rad)	Side Lobe Level (dB)	ε_t	HP (rad)	Side Lobe Level (dB)	ε_t
−8	0.398	$1.12\,\frac{\lambda}{2a}$	−21.5	0.942	$1.14\,\frac{\lambda}{2a}$	−24.7	0.918
−10	0.316	$1.14\,\frac{\lambda}{2a}$	−22.3	0.917	$1.17\,\frac{\lambda}{2a}$	−27.0	0.877
−12	0.251	$1.16\,\frac{\lambda}{2a}$	−22.9	0.893	$1.20\,\frac{\lambda}{2a}$	−29.5	0.834
−14	0.200	$1.17\,\frac{\lambda}{2a}$	−23.4	0.871	$1.23\,\frac{\lambda}{2a}$	−31.7	0.792
−16	0.158	$1.19\,\frac{\lambda}{2a}$	−23.8	0.850	$1.26\,\frac{\lambda}{2a}$	−33.5	0.754
−18	0.126	$1.20\,\frac{\lambda}{2a}$	−24.1	0.833	$1.29\,\frac{\lambda}{2a}$	−34.5	0.719
−20	0.100	$1.21\,\frac{\lambda}{2a}$	−24.3	0.817	$1.32\,\frac{\lambda}{2a}$	−34.7	0.690